COMSOL
CONFERENCE
2023 MUNICH

Investigations on talik formation during changes to cold climates

K.-P. Kröhn

Department of Repository Safety, GRS gGmbH, Braunschweig, Germany.

Abstract

In the context of the safety assessment for deep geological disposal of radioactive waste, groundwater flow must be well characterized not only under the presently warm climate but also under permafrost conditions. The latter have occurred several times over present-day Germany during the same period of time in the past for which safety is demanded legally in the future. Freezing of the underground during cold climates appears to be advantageously at a first glance because, by and large, it shields the biosphere from possibly contaminated groundwater from repository depths. However, it is known from present permafrost regions that unfrozen zones exist under large surface waters such as lakes or rivers, called taliki, that penetrate the permafrost and may even connect the surface hydraulically with deep aquifers.

While it should be imperative to understand the conditions under which taliki are forming, very little is actually known in that respect. It is thus that the present work is intended to provide a starting point for investigations concerning the circumstances for talik forming by means of numerical modelling as this method allows for comparatively quick variations of possible influence quantities. A stringent mathematical framework has already been worked on so that setting up a first concrete numerical model and related results are presented in the present paper.

Keywords: groundwater flow, permafrost, talik, radioactive waste

Introduction

Over the past million years, several cold ages have occurred and thereby caused permafrost conditions basically all over the present area of Germany. Since in Germany the safety of a nuclear waste repository legally needs to be investigated for a period of one million years [1], the ground freezing effect of permafrost must be included in the long-term safety assessment with respect to the groundwater flow system.

While in principle the ground freezing in the upper geosphere should shield the biosphere from possibly contaminated groundwater in deeper aquifers, there is the phenomenon of taliki (singular: talik) which is well-known from present-day permafrost regions. Taliki are locally unfrozen zones that can reach through the whole permafrost-induced frozen ground and thus may form a hydraulic shortcut between deep aquifers and the surface, thereby possibly concentrating the flux of harmful substances. The conditions for the forming of taliki and their long-term stability – highly important for the safety assessment – are largely unknown, though. It is known, however, that taliki exist preferably under large surface waters such as lakes or rivers (e.g. [2]) as indicated in Figure 1.

Due to their nature, taliki are difficult to detect and to observe in-situ. And even if the costly effort to investigate them is actually undertaken (e.g. [3]), the results refer only to the present conditions of their existence.

It is thus that alternatively numerical investigations will be used here that allow for comparatively quick and encompassing variations of a baseline model setup. This method is believed to help considerably identifying favorable conditions for forming a talik.

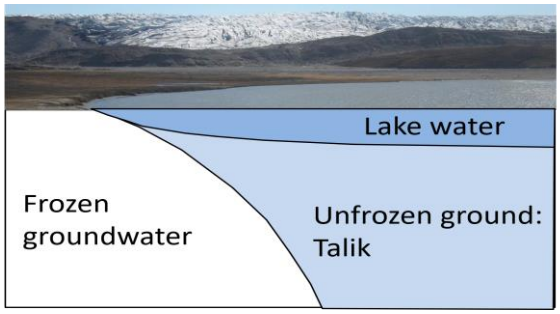

Figure 1. Idealized vertical cross-section through a lake under permafrost conditions.

Physical framework

A systematic numerical investigation of groundwater flow under permafrost conditions needs only a few physical features to be considered which are (cp. [4]):

- advective groundwater flow that occurs in porous media even at subzero temperatures,
- heat flow in porous media by convection and conduction, and
- temperature dependent phase change of pore water.

Groundwater flow above 0 °C will be treated here as single-phase flow in a porous medium. However, where the temperature falls below the freezing temperature, a temperature-dependent fraction of water undergoes a phase change from liquid to solid, thus forming ice in the pore space. In effect, groundwater flow under permafrost conditions thus involves up to three phases: water, ice and the solid matrix.

For the purpose at hand, is assumed that neither ice nor the matrix are subject to movement or deformation. In this case, flow of the remaining

supercooled water can be described analogously to the classic unsaturated flow setup where the movement of the air is neglected. Furthermore, constant porosity and thus no water storage by the matrix follows from this assumption.

Two effects need additionally to be taken into consideration where phase changes of the water are concerned. One is the different density of water and ice at the same temperature which is about 10 % lower for ice than for water and leads to a volumetric expansion during freezing. The second is the latent heat of freezing that is set free during freezing of water and is required for melting ice.

For heat flow only isotropic and homogeneous media are considered. At that, a local thermal equilibrium between all phases involved is assumed. As the saturation vapour pressure increases rapidly with depth, boiling of the groundwater can be excluded.

Mathematical framework

Two balance equations describing the above outlined mass and heat flow processes have stringently been developed in [4]. They were derived by starting out with general balance equations separately for each phase that were subsequently combined by adding.

Four constitutive equations (CE) were required to reify the balance equations:

- the generalized Darcy's law for flow that relates hydraulic pressure to flow velocity including gravity,
- a soil freezing characteristic curve (SFCC) relating temperature to the water saturation in the pore space,
- a relative permeability relation depending on the water saturation,
- Fourier's laws relating temperature to heat flux.

Depending on the phase in question, up to four equations of state (EOS) are required: density, viscosity, thermal conductivity and heat capacity. All EOS depend on temperature, the EOS for water depend also on pressure.

In contrast to the CE that are characteristic for a specific porous medium, accurately derived EOS are in principle valid once for all as they describe the properties of pure substances. However, if used in the framework of a numerical code, it is essential that the primary variables upon which the EOS depend, in this case hydraulic pressure and temperature, do not leave the range of validity of the EOS in use. It should thus be good modelling practice to check this either during the simulation run or afterwards properly.

Model definition

The model definition is given here in short. A more detailed discussion can be found in [5].

Model domain

A lake on a granitic formation is considered in an axisymmetric geometry where the symmetry axis passes through the middle of the lake. As a first approach the lake is assumed to have a diameter of 100 m and a maximum depth of 25 m.

Initial and boundary conditions

The hydraulic initial and boundary conditions are straightforward as they simply refer to the initial hydrostatic pressure as indicated in Figure 2. The lateral boundary conditions are chosen for the sake of simplicity to be of the no-flow type. This requires a minimum distance of the lateral surface from the symmetry axis to avoid an artificial increase of pressure and heat at this location. Based on preliminary modelling this distance is chosen to be 1000 m n the model.

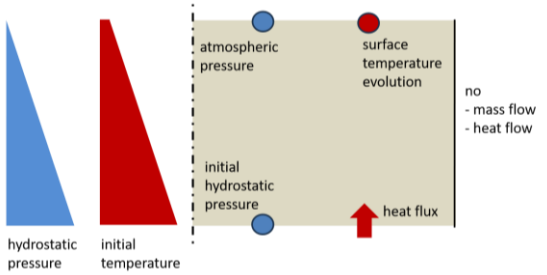

Figure 2. Hydraulic and thermal initial and boundary conditions for the model; after [5].

By contrast, the thermal boundary conditions required more investigative work (cp. [5]). Heat flux from earth's interior is basically constant over the period of one million years and an average over Germany amounts to 78 mW/m². At the top, the temperature evolution over present-day Germany has been reconstructed based on ice cores of deeply drilled boreholes from Antarctica as depicted in Figure 3. A strongly simplified polygon overlaying the reconstructed data is supposed to characterize the climate cooling in the model that led to the last glacial maximum. This simplified temperature evolution is assigned to the top boundary of the model. For the initial thermal conditions, equilibrium of the temperature at the top with the heat flux from the bottom is assumed.

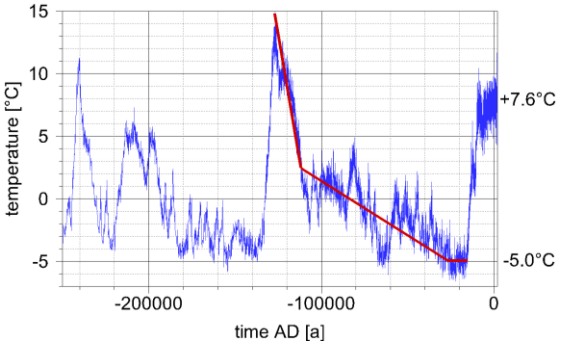

Figure 3. Reconstruction of air temperature evolution over present-day Germany; from [5].

Realization in COMSOL

The continuity equation from [4] reads

$$\left[S_w \Phi \frac{\partial \rho_w}{\partial p}\right]\frac{\partial p}{\partial t} - \nabla \cdot \left(\rho_w \frac{k_{rw}}{\eta_w}\boldsymbol{k} \cdot (\boldsymbol{\nabla} p - \rho_w \boldsymbol{g})\right) = - \left[\Phi(\rho_w - \rho_i)\frac{\partial S_w}{\partial T} + S_w \Phi \frac{\partial \rho_w}{\partial T} + S_i \Phi \frac{\partial \rho_i}{\partial T}\right]\frac{\partial T}{\partial t} \quad [1]$$

An explanation of the symbols can be found at the end of the paper.

The first term on the left-hand side and the second term on the right-hand side refer to compressibility and thermal expansion of the water which are handled together in COMSOL. Thermal expansion of the ice is addressed with the third term on the right-hand side and the volumetric changes due to phase changes are taken care of by the first term on the right-hand side. This has been transferred into the COMSOL interface "Darcy's law" accordingly. In an analogous but much more complex way, the same procedure was also applied to the balance equation for heat that is realized in the "Heat transfer in porous media" interface.

As for the CE, a temperature-dependent relative permeability k_r has been added and multiplied with the absolute permeability in Darcy's law. It is defined as

$$k_r = \max\left(10^{-6}, {S_w}^3\right) \quad [2]$$

and is related to the water saturation S_w that in turn is given by the SFCC as depicted in Figure 4. The SFCC is based on the smoothed Heaviside function flc2hs provided by COMSOL with continuous second order derivatives. To represent the phase change from water to ice, the phase change material node under the heat flow interface was applied, but modified in the equation view mode to allow for a varying width of the transition zone (this had not been possible in version 6.0 of COMSOL). The curve eventually used is point-symmetric with the symmetry point at -1 °C and a transition range of 1 K to each side.

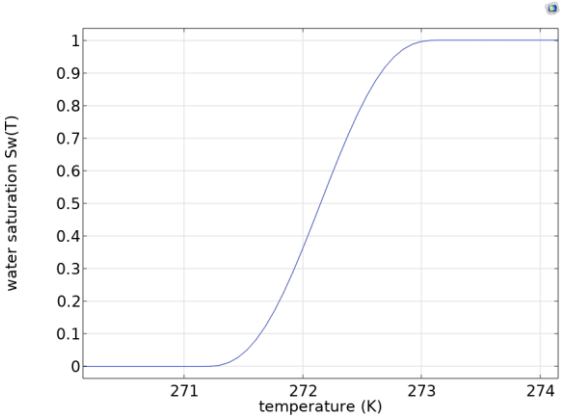

Figure 4. Water saturation as a function of temperature.

Quite some effort went into new simplified but accurate EOS for water as the range of validity for the ones provided by [4] proved to be insufficient. These had been derived for temperatures between -20 °C and +20 °C and a hydraulic pressure of up to 10 MPa making them valid for depths down 1000 m. The temperature changes introduced at the top of the model reached the originally envisioned maximum depth in less than 10,000 years, though. The new simplified EOS were valid up to +60 °C and up to 20 MPa covering depths down to 2000 m. They are described in detail in the appendix. However, even 2000 m was not deep enough.

Therefore, it was decided not to enlarge the range of validity again but to extend the model downwards to 6000 m depth for the thermal simulation since the EOS for the rock were valid up to 200 °C to begin with. As an approximation, only rock with a porosity of 0 was considered in the extended section. This model setup is depicted in Figure 5.

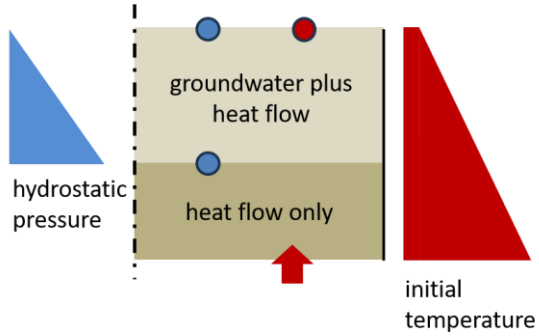

Figure 5. Final model setup.

To allow for a certain flexibility of the model geometry, all characteristic lengths are parameterized. This applies in particular to the shape of the axisymmetric lake which is illustrated in Figure 6.

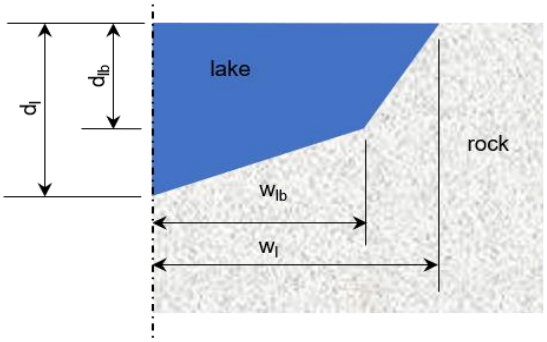

Figure 6. Parameterization of the lake geometry.

Characteristic parameters for the rock were chosen to coincide with those of the crystalline rock at the Grimsel Test Site in the Swiss Alps (e.g. [6]). The lake was ad hoc treated as porous medium with a permeability and a porosity as high as 10^{-11} m² and 99 %, respectively.

Simulation Results / Discussion

The results of the first model run provided confirmation of the modelling framework as

significant features were qualitatively reproduced as expected. The first result in this respect is that of thermal insulation of the underground by the lake against cooling. In Figure 7, a vertical cross-section of the model is shown depicting the total heat flux after 2000 years model time. Heat flow is visualized by means of a vector field, a colour plot representing the absolute value of the flux, and path lines.

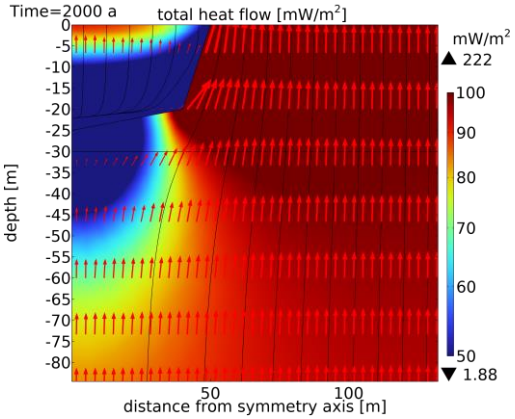

Figure 7. Total heat flux in the vicinity of the lake after 2000 years.

As water and to a somewhat lesser extent also ice is much less conductive for heat than the rock, the heat flux over the top boundary is lower via the water in the lake than via the open granitic ground. As a result, heat flow is deflected by the lake. This indicates a slowing of cooling in the area of the lake and thus higher temperatures in the lake and its vicinity as shown in Figure 8.

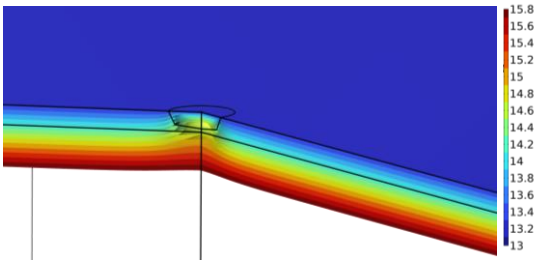

Figure 8. Temperature distribution in the vicinity of the lake after 2000 years.

This temperature anomaly that is caused by the large body of water, lets water and the ground in its vicinity freeze a little later than the area further away from the lake. A temperature of 0°C is reached in the model after little more than 43,000 years. After 60,000 years, the 90 % isoline for water saturation, equivalent to a fraction of 10 % of ice in the pore space, has not yet reached the bottom of the lake at 25 m but has already gone down to about 33 m further away from the lake as depicted in Figure 9.

Freezing increases its intensity over the following almost 70,000 years. During this time, the freezing front advances down to a depth of about 150 m. At the same time, the front becomes basically horizontal. Figure 10 shows the water saturation and the vector field of groundwater flow at the end of the simulation.

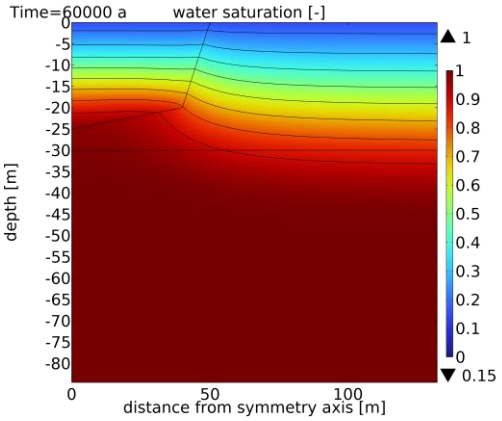

Figure 9. Water saturation in the vicinity of the lake after 60,000 years.

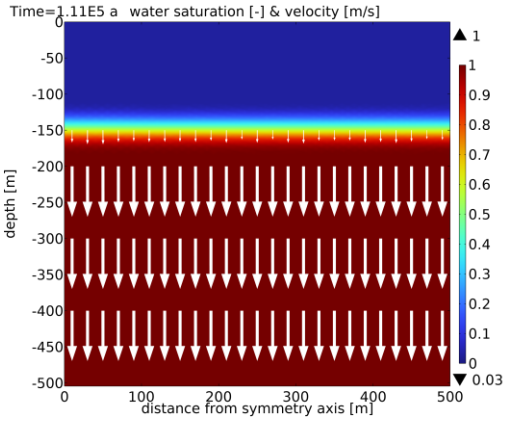

Figure 10. Water saturation and flow velocity at the end of simulation (111,500 years).

Apparently, groundwater flow is only driven by the freezing of water as the less dense ice displaces the remaining water. The resulting flow velocity is consequently extremely low lying in the range of tens of micrometers per year, so that heat flow is essentially conductive in this model. Density variations with depth due to changing of pressure and temperature are not enough to initiate convective flow and a concurrent heat transport.

Conclusions

Much effort has been invested in the development of an accurate mathematical framework for modelling groundwater flow under permafrost conditions. The same applies also to the choice of appropriate conditions and parameters for the first referring numerical model.

The results of this first model inspire confidence into the modelling framework as a whole. Significant features were qualitatively reproduced as expected. This concerns the insulating properties of large volumes of water as in lakes as well as the ability of the model to reproduce not only freezing of the ground but also the concurrent displacement of pore water.

The first model would have been an even greater success if it had been showing signs of talik

formation. This was expressively not the case. The model is thermally dominated by heat conduction. It didn't show signs of convective heat flow that is suspected to keep taliki up. However, the sensitivity of the processes involved leaves a wide field open for further analysis.

List of symbols

S_w	-	water saturation [-]
Φ	-	porosity [-]
ρ_w	-	density of water [kg/m³]
ρ_i	-	density of ice [kg/m³]
p	-	hydraulic pressure [Pa]
t	-	time [s]
k_{rw}	-	relative permeability [-]
η_w	-	viscosity [Pa s]
$\boldsymbol{k}$	-	permeability tensor [m²]
$\boldsymbol{g}$	-	vector of gravitational acceleration [m/s²]
T	-	temperature [K]

References

[1] Deutscher Bundestag, *Gesetz zur Suche und Auswahl eines Standortes für ein Endlager für hochradioaktive Abfälle (Standortauswahlgesetz - StandAG)*, decision of the Deutscher Bundestag, 2017.

[2] G. Delisle, "Numerical simulation of permafrost growth and decay," *Journal of Quarternary Science*, vol. 13, no. 4, pp. 325-333, 1998.

[3] J. Harper, A. Hubbard, T. Ruskeeniemi, L. Claesson Liljedahl, A. Lehtinen, A. Booth, D. Brinkerhoff, H. Drake, C. Dow, S. Doyle, J. Engström, A. Fitzpatrick, S. Frape, E. Henkemans, N. Humphrey, J. Johnson, G. Jones, I. Joughin, K. E. Klint, I. Kukkonen, B. Kulessa, C. Landowski, K. Lindbäck, M. Makahnouk, T. Meierbachtol, T. Pere, K. Pedersen, R. Pettersson, S. Pimentel, D. Quincey, E.-L. Tullborg and D. van As, "The Greenland Analogue Project, Yearly Report 2010," report R-11-23, Svensk Kärnbränslehantering (SKB), Stockholm, 2011.

[4] K.-P. Kröhn, "Basics for groundwater flow under permafrost conditions in the context of radioactive waste storage," FKZ 02 E 11809A (BMWi), Gesellschaft für Anlagen- und Reaktorsicherheit (GRS) gGmbH, report GRS-707, Braunschweig, 2023.

[5] K.-P. Kröhn, "Groundwater flow under permafrost conditions and talik formation," in *12th International Conference on Permafrost*, White Horse, Yukon, Canada, 2024 (under review).

[6] A. Gens, L. d. N. Guimaraes, A. Garcia-Molina and E. Alonso, "Factors controlling rock–clay buffer interaction in a radioactive waste repository," *Engineering Geology*, vol. 64, p. 297 – 308, 2002.

[7] K.-P.Kröhn, "State Variables for Modelling Thermohaline Flow in Rocks," FKZ 02 E 10336 (BMWi), Gesellschaft für Anlagen- und Reaktorsicherheit (GRS) gGmbH, Braunschweig, 2010.

[8] The International Association for Properties of Water and Steam, "Revised Guideline on Thermodynamic Properties of Supercooled Water," 2015. [Online]. Available: http://www.iapws.org. [Accessed 2023].

[9] The International Association for Properties of Water and Steam, "Revised Release on the IAPS Formulation 1985 for the Viscosity of Ordinary Water Substance," 2003. [Online]. Available: http://ww.iapws.org. [Accessed 2023].

[10] The International Association for the Properties of Water and Steam, "Revised Release on the IAPWS Formulation 2003 for the Viscosity of Ordinary Water Substance," 2008. [Online]. Available: http://www.iapws.org. [Accessed 2023].

[11] The International Association for Properties of Water and Steam, "Revised Release on the IAPWS Formulation 2011 for the Thermal Conductivity of Ordinary Water Substance," 2011. [Online]. Available: http://www.iapws.org. [Accessed 2023].

Acknowledgements

The author gratefully acknowledges the funding of the theoretical investigations under contract no. 02 E 11941 with the German Federal Ministry for the Environment, Nature Conservation, Nuclear Safety and Consumer Protection (BMUV).

Appendix Equations of state for water

Extending the range of validity for the equations of state (EOS) to -20 °C < T < +60 °C for temperature and to 0.1 < p < 20 MPa for hydraulic pressure concerns only the water phase. Ice and rock are assumed to depend only on temperature so that these EOS are not affected by an extension of the valid pressure range. As for an increased upper limit for the temperature, ice is also not affected since it exists only below 0 °C. The same applies by analogy to the rock as the EOS for the rock are already valid up to +200 °C [7].

What remains to be addressed are therefore density, viscosity, thermal conductivity and heat capacity of the water. The EOS at atmospheric pressure were derived first, then modifications accounting for the influence of pressure were added. All four EOS are then compared graphically with reference formulations from the International Association for the Properties of Water and Steam (IAPWS).

Water density $\rho_0(T)$ at atmospheric pressure reads

$$\begin{aligned}\rho_0(T) = \; & 999.974 \\ & - (0.0075+0.001*(\text{sign}(T')+1)/2)*T'^2 \\ & +(1.5e\text{-}4 \;\; -7.e\text{-}5*(\text{sign}(T')+1)/2)*T'^3 \\ & - 0.0045*((\text{sign}(\check{T})+1)/2)*\check{T}^2\end{aligned} \qquad \text{[A1]}$$

with

$$T' = T-4$$

$$\check{T} = T-30$$

To include the influence of pressure, Equation A1 is modified to Equation A2.

$$\begin{aligned}\rho(T,p) = \; & \rho_0(T) \\ & +(\rho_0(T)*0.0025-0.0205*T \\ & +5e\text{-}4*T^2)*(p-0.1)/4.9 \\ & -(p/27)4 \\ & -(0.00048*p)*(((\text{sign}(T-20)+1)/2) \\ & *(T-20))^{1.6}\end{aligned} \qquad \text{[A2]}$$

The reference formulation from [8] for the temperature- and pressure-dependent density of water is rather complex but also covering a vast range of temperatures and pressures. The graphic comparison of Equation A2 with this reference in Figure A1 shows without further analysis that the match can be considered to be quite satisfying.

The reference formulations of [9], [10] on the viscosity can be approximated by the expression in Equation [A3]:

$$\begin{aligned}\eta(T,p) = \; & 0.00037 \\ & +6.8e\text{-}9*|T-100|^{2.6} \; +1.8e\text{-}8 \\ & *((-(\text{sign}(T-30)-1)/2)*(30-T))^{2.9} \\ & +1.7e\text{-}7*(((\text{sign}(T)-1)/2)*T)^{2.8} \\ & -2.853e\text{-}4*(p-0.1)/19.9*(1-(T+20)/80)^6\end{aligned} \qquad \text{[A3]}$$

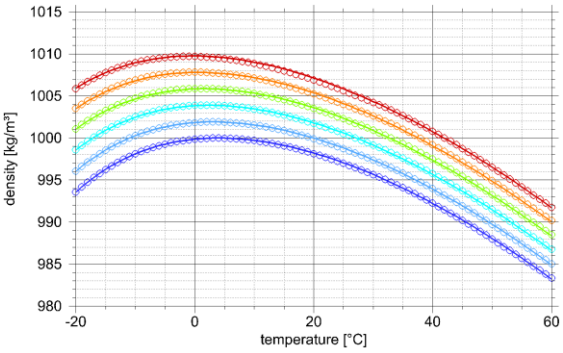

Figure A1. Density of water; lines – reference formulation; symbols – present formulation; colours: blue – 0.1 MPa, light blue – 4 MPa; turquoise – 8 MPa; light green – 12 MPa; orange – 16 MPa; red – 20 MPa.

According to the graphical comparison of the reference formulation and Equation A3 in Figure A2, the match of the curves is again satisfying. Note that the influence of pressure on water viscosity is apparently very small.

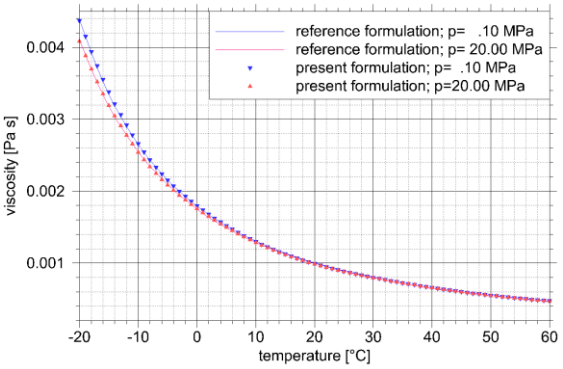

Figure A2. Viscosity of water.

In case of the thermal conductivity, the reference formulations come from [11]. The present formulation is given as Equation A4, the graphic comparison with the reference formulation in Figure A3.

$$\begin{aligned}\lambda(T,p) = \; & 0.55559 \\ & + 0.00270*T\text{-}3e\text{-}5*(T+1.5)^2 \\ & +2.8e\text{-}7*(T-0.5)^3 \\ & -1.9e\text{-}5*(((\text{sign}(T-35)+1)/2)*(T-35)*1)^2 \\ & + (p-0.1)/19.9*(0.02079*|(1-(T+20)/80)|^{2.7} \\ & + 0.01017 \; *|(v1+20)/80|^{0.4})\end{aligned} \qquad \text{[A4]}$$

The simplified formulation for the heat capacity of water has been particularly tricky as it required a pressure dependent starting point (T',p') from which the heat capacity curves evolve. The graphic comparison of the present formulation Equation A5 with the reference formulation from [8]is shown in Figure A4. The starting points are depicted as large diamonds.

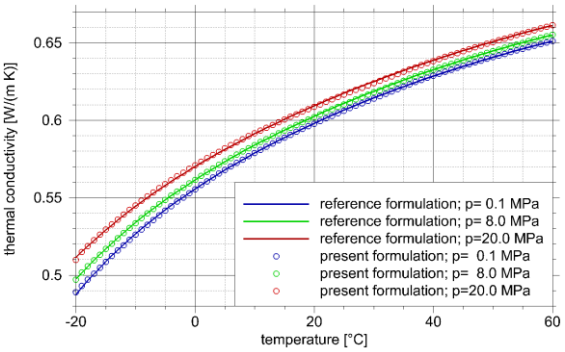

Figure A3. Thermal conductivity of water; lines – reference formulation; symbols – present formulation; colours: blue – 0.1 MPa, turquoise – 8 MPa; orange – 16 MPa; red – 20 MPa.

$$c(T,p) = p' - ((\mathrm{sign}(\check{T})-1)/2)*0.00132 *(\exp(|\check{T}|*(0.086+0.05*((p-0.1)/20)^{2.7}))-1) +4e\text{-}5*((\mathrm{sign}(\check{T})+1)/2)*|\check{T}|^{1.5}$$

with [A5]

$$T' = 40-0.335*p^{1.5}$$

$$\check{T} = T-T'$$

$$p' = 4.1786-0.00195*p^{1.1}$$

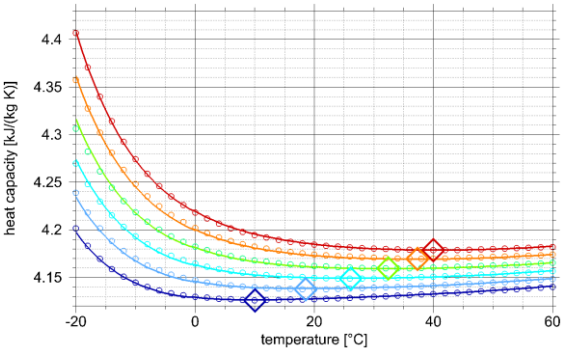

Figure A4. Heat capacity of water; lines – reference formulation; symbols – present formulation; colours: blue – 0.1 MPa, light blue – 4 MPa; turquoise – 8 MPa; light green – 12 MPa; orange – 16 MPa; red – 20 MPa.